Journal of Interdisciplinary Mathematics
ISSN: 0972-0502 (Print), ISSN: 2169-012X (Online)
Vol. 26 (2023), No. 3, pp. 483–503
DOI : 10.47974/JIM-1676

Illustration of free convection tangent hyperbolic fluid in conjunction with magnetic field within a microchannel

P. K. Pattnaik *
Department of Mathematics
Odisha University of Technology and Research
Bhubaneswar 751029
Odisha
India

S. R. Mishra †
Department of Mathematics
Siksha 'O' Anusandhan (Deemed to be University)
Bhubaneswar 751030
Odisha
India

Priya Mathur §
Department of Mathematics
Poornima Institute of Engineering & Technology
Jaipur 302022
Rajasthan
India

Geetanjali Pradhan ‡
Department of Mathematics
Odisha University of Technology and Research
Bhubaneswar 751029
Odisha
India

* *E-mail:* papun.pattnaik@gmail.com (Corresponding Author)
† *E-mail:* satyaranjan_mshr@yahoo.co.in
§ *E-mail:* priya.mathur@poornima.org
‡ *E-mail:* geetanjalipradhan65@gmail.com

Dinesh Goyal [@]
Department of Computer Science & Engineering
Poornima Institute of Engineering & Technology
Jaipur 302022
Rajasthan
India

Abstract

This article investigates the physical interpretation of the magnetic field on the free convection of hyperbolic tangent fluid within a microchannel. The radiating heat through the permeable surface, dissipative heat and the additional heat source experience an important role. The interaction of magnetic dissipation and Darcy-dissipation can be neglected as the flow is supposed to be affected by including a magnetic field and the medium's permeability. The dimensional form of the designed model is converted to its corresponding non-dimensional form for the use of the similarity variables. Further, these are handled using an approximate analytical technique known as the Adomian decomposition method. The physical behaviour of certain characterizing parameters on the non-Newtonian flow phenomena is exhibited and displayed graphically, and the tabular form is used for the numerical simulation of the rate coefficients.

Subject Classification: *76-10 Mathematical Modeling and Simulation for Problems pertaining to fluid Mechanics.*

Keywords: *Tangent hyperbolic fluid, Dissipative heat, Thermal radiation, Heat source, Adomian decomposition method.*

1. Introduction

In recent days the applications of nanofluids have been vital for the various design models obtained by diffusing nanoparticles, likely copper, aluminium, etc., into the base liquids, i.e., water, oil, etc. Nanofluids exhibit completely new properties when the base fluid is used as a solvent and the nanoparticles are used as solutes. Nanofluids are nanotechnology-based transfer fluids which are useful for cooling and related technology. More importantly, the heat transport phenomena enhanced in the case of nanofluid compared to the base liquids. Choi et. al. [1] input the knowledge of such fluids in 1995 as "Nanofluids" as high thermal conductive. This theoretical study uses Hamilton and crosser model to explain copper nanomaterials in water. Finally, in conclusion, the authors have noted some points about the pumping performance of heat exchangers. Hayat

[@] *E-mail:* **dinesh.goyal@poornima.org**

et. al. [2] discussed elaborately the flow of magnetic nanofluids between two parallel discs. The authors worked on the reactions which follows homogeneous-heterogeneous criteria in a ferrofluid flow affected by a disk which always rotates. They have mathematically analyzed the values of physical quantities i.e., skin friction and Nussult number, considering the nanofluid prepared from the combination of water magnetite-Fe3O4 as solute. The role of homogeneous and heterogeneous reactions has been discussed for the concentration distribution, showing their effectiveness in enhancing the profiles.

Further, the rate coefficients are presented for the various components associated with the model. Sheikholeslami et. al. [3] have extensively discussed the influence of nanofluid flow, impacting the presence of forced convection heat transfer through a porous cavity. To simulate the stream function, CVFEM was used, and the conclusion was convective heat improved with an augmented Darcy and Reynolds number. Uniform mass flux has a great role on the behaviour of natural convection which is deployed by Chamkha et. al. [4]. They have proposed a nanofluid which is non-Newtonian in nature and flows via vertical cone embedding within a permeable medium and finally employed the Keller box method for the solution of the designed model. The important impactness of thermophoresis and Brownian motion can be visualized from the conclusive remark obtained by the authors. Chamkha et. al. [5] studied numerical solutions of MHD-free convection flow of nanofluids. The tri-diagonal implicit FDM (finite difference method) was used to the problem and is seen that, the results are strongly agreed with previous results.

Convection heat transfer is the transfer of heat between two bodies due to the flow of fluid or gas. Energy can be transferred both by heat conduction and macroscopic motion of the fluid. The convection of heat transfer process is very important in porous insulation cooling, rotating electric windings etc. A water-based liquid composed of magnetite-Fe_3O_4 as a nanoparticle was prepared by Guo et. al. [6] in the year 2015. Many researchers have discussed the behaviour of the flow that occurs between two rotating disks which have different velocities. The behaviour of velocity slip and the convective boundary condition for the heat transport phenomenon is useful for comparative work with the previous study. Sheikholeslami et. al. [7-9] discussed different geometry in the study of the nanofluid flow behaviour by considering various thermophysical properties. In their investigation, one of the important aspects is the role of magnetic parameters on the flow of Fe_3O_4 water-based nanofluid through parallel plates associated with the Lorentz force. They have employed both analytical as well as numerical techniques for mathematical analysis. In particular, computation is carried out by deploying the differential transform method and FEM. Bhatti et. al. [10] comprehended that the impact of Darcy dissipation could not be ignored under certain circumstances when a fluid flow through a permeable medium. With these assumptions mentioned earlier, authors have carried out their investigation by considering the effect of Darcy dissipation and the chemical reaction, and other SLLM methods are helpful for the solution of transformed flow phenomena. Jena et. al. [11] considered a comparative discussion using water and kerosene as traditional fluids with copper as nanoparticles.

Calculations are performed for different profiles to compare both nanofluids, and it is concluded that the Cu-kerosene nanofluid is dominated by Cu-water nanofluid for the velocity and temperature profiles. Recently, Jena et. al. [12] proposed a numerical solution behaviour for nanofluid flow through parallel plates by implementing the RK4 (4^{th} order Runge-Kutta) method by considering shooting technique. Further, Haq et. al. [13] worked on the natural convection of a cavity which contains water-based copper oxide nanofluid. Here, one important and interesting case was discussed, which is explained by treating the bottom as heated, and the top as adiabatic, whereas the remaining parts became cold. A a bidirectional exponentially stretching surface has been considered in the work of Ahmad et. al. [14] to execute the nanofluid flow. Here, they have proposed Maxwell models for the formulation of their model. Ramesh et. al. [15] investigated a numerical behaviour of solution obtained from the study of the flow at the stagnation point (Maxwell fluid) concerning an expanding film containing nanoparticles. As a conclusive remark, the velocity profile is enhanced due to the higher Maxwell parameter, while the temperature and concentration profiles goes reverse to it. Bhatti et. al. [16] illustrated the irreversibility process's behaviour for considering the Eyring-Powell nanofluid model for enhanced thermal properties. In this study, the inclusion of the Brownian motion gives a convergent behaviour for the nanoparticle concentration profile.

Further research on this topic can be found in references [17-24]. Mishra et. al. [25] explored the influence of exponential heat source on the nano-micropolar fluid over a convectively heated elongated plate. Barik [26] studied the numerical results of multiple slips affecting the MHD nanofluid flow with his colleagues. Mishra et. al. [27, 28] worked to convection heat in micropolar fluids with different heat sources. Many researchers [29-32] in the last decade focused on nanofluids and their heat transfer properties with various mathematical approaches. Chamkha et.

al. [33, 34] studied nanofluids' heat and mass transport properties within a permeable media. Cogley [35] initiated the importance of thermal radiation on a time-dependent MHD fluid flow [36-40].

Insight to the aforesaid properties and description presented in the various literature, the present aim reveals the significant characteristic of the free convection of tangent hyperbolic nanofluid flow past a parallel channel in the presence of dissipative heat and thermal radiation. The electrically conducting nanofluid flow through a permeable medium is equipped with a heat source, and the effect of Brownian motion and thermophoresis enriches the flow phenomena. Because of the different applications in industries depending upon the shape of the final product, the role of a chemical reaction is also important in this investigation. Finally, the designed complex nonlinear problem is solved analytically using the Adomian Decomposition Method.

2. Mathematical model

The present study deals with the characteristic of the flow of a tangential hyperbolic fluid via a horizontal microchannel considering the free convection effect. The channel is composed of two parallel plates separating each other with infinite lengths (Figure 1). A uniform transverse magnetic field of strength B_0 is imposed in the normal direction of the flow. In modelling the physical phenomenon, the effects of various parameters on the flow profiles for the effect of velocity slip and convective boundary conditions are considered. With these assumptions, the model is designed as follows;

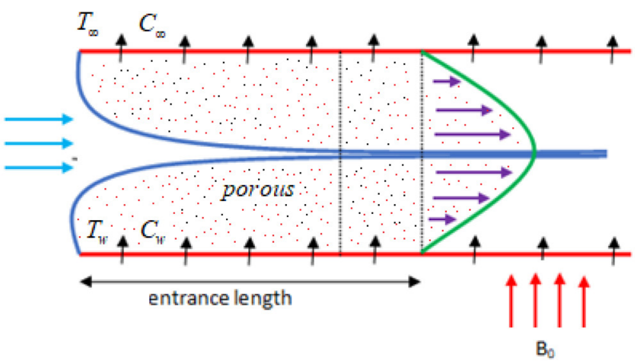

Figure 1

Schematic diagram of the flow

$$\rho v_0 \frac{df}{dy} = -\frac{dp}{dx} + \mu(1-n)\frac{d^2 f}{dy^2} + \sqrt{2} n\mu\Gamma \frac{df}{dy}\frac{d^2 f}{dy^2} - \left(\sigma B_0^2 + \frac{\mu}{k_p^*}\right) f + \rho g(\beta_T (T - T_\infty) + \beta_C (C - C_\infty)), \quad (1)$$

$$(\rho c_p) v_0 \frac{dT}{dy} = k\frac{d^2 T}{dy^2} + \mu\left(\frac{df}{dy}\right)^2 + \left(\sigma B_0^2 + \frac{\mu}{k_p^*}\right) f^2 - \frac{\partial q_r}{\partial y} + Q_0 (T - T_\infty) + (\rho c_p)_{np} D_B \frac{\partial T}{\partial y}\frac{\partial C}{\partial y} + (\rho c_p)_{np}\frac{D_T}{T_\infty}\left(\frac{\partial T}{\partial y}\right)^2 \quad (2)$$

$$D_B \frac{d^2 C}{dy^2} + \frac{D_T}{T_\infty}\frac{d^2 T}{dy^2} = K^*(C - C_\infty) \quad (3)$$

$$\begin{aligned} &f = S_f f'(y), k_f T'(y) = h_c (T - T_w), C = C_\infty \quad \text{at } y = 0, \\ &f = -S_f f'(y), k_f T'(y) = -h_c (T - T_w), C = C_w \quad \text{at } y = a \end{aligned} \quad (4)$$

where the usual notations for the variables and the constants are presented in the nomenclature section. Radiant heat flux (see [35]) is used as,

$$\frac{\partial q_r}{\partial y} = 4(T - T_\infty) I^*, \quad (5)$$

with

$$I^* = \lim_{\lambda\to\infty} \int_0^\lambda \left(\frac{\partial e_{b\lambda}}{\partial T}\right)_w K_{\lambda w} d\lambda \quad (6)$$

mean absorption coefficient $(K_{\lambda w})$ and Planck's function $(e_{b\lambda})$.

Non-dimensional quantities (see [36, 37]) are used to prepare dimensionless equations as follows,

$$f = \frac{\upsilon}{a} F, y = a\xi, T = T_\infty + \theta(T_w - T_\infty), C = C_\infty + \phi(C_w - C_\infty), \quad (7)$$

After using the above said dimensionless quantities, eqns. (2-4) become

$$(1-n)F'' + nWeF'F'' - \operatorname{Re} F' - (M + Da)F + \lambda_1\theta + \lambda_2\phi + P = 0, \quad (8)$$

$$\theta'' - \Pr\operatorname{Re}\theta' + \Pr(EcF'^2 + (M + Da)EcF^2 + Nb\theta'\phi' + Nt\theta'^2 + (S + I)\theta) = 0, \quad (9)$$

$$\phi'' + \frac{Nt}{Nb}\theta'' - K\,Le\Pr\phi = 0, \quad (10)$$

$$\begin{aligned} &F = S_v F', \theta' = B_i(\theta - 1),\ \phi = 0 \quad \text{at} \quad \xi = 0, \\ &F = -S_v F', \theta' = -B_i(\theta - 1),\ \phi = 1 \quad \text{at} \quad \xi = 1. \end{aligned} \tag{11}$$

$$\begin{aligned} &M = \frac{\sigma a^2 B_0^2}{\mu}, Da = \frac{a^2}{\upsilon k_p^*}, We = \frac{\sqrt{2}\Gamma\upsilon}{a^2}, \mathrm{Re} = \frac{a v_0}{\upsilon}, \lambda_1 = \frac{\beta a^3}{\upsilon}(T_w - T_\infty), \\ &\lambda_2 = \frac{\beta a^3}{\upsilon}(C_w - C_\infty), \mathrm{P} = -\frac{a^3\rho}{\mu^2}\frac{dp}{dx}, \mathrm{Pr} = \frac{\mu c_p}{k}, S = \frac{a^2 Q_0}{\mu c_p}, I = \frac{4\upsilon^2 I^*}{\kappa v_0^2}, \\ &Ec = \frac{\upsilon^2}{a^2 c_p (T_w - T_\infty)}, S_v = \frac{S_f}{a}, B_i = \frac{a h_c}{k}, K = \frac{K^* a^2}{\upsilon}. \end{aligned} \tag{12}$$

We, the Weissenberg number, and I, the Radiation parameter.

3. Aspects of physical quantities of engineering interest

At both the lower and upper ends the rate coefficients of plates are calculated as follows:

$$\left.\begin{aligned} &Cf_a = \frac{a^2}{\upsilon}((1-n)f'(y) + \sqrt{0.5}n\Gamma f'^2(y))_{y=a} \\ &Nu_a = -\frac{a}{T_w - T_\infty}(T'(y))_{y=a}, Sh_a = -\frac{a}{C_w - C_\infty}(C'(y))_{y=a} \end{aligned}\right\} \tag{13}$$

$$\left.\begin{aligned} &Cf_0 = ((1-n)F'(\xi) + 0.5nWeF'^2(\xi))_{\xi=0} \\ &Nu_0 = -(1+Nr)(\theta'(\xi))_{\xi=0}, Sh_0 = -(\phi'(\xi))_{\xi=0} \end{aligned}\right) \tag{14}$$

$$\left.\begin{aligned} &Cf_1 = ((1-n)F'(\xi) + 0.5nWeF'^2(\xi))_{\xi=1} \\ &Nu_1 = -(1+Nr)(\theta'(\xi))_{\xi=1}, Sh_1 = -(\phi'(\xi))_{\xi=1} \end{aligned}\right) \tag{15}$$

4. Proposed Method (Adomian Decomposition Method (ADM))

The transformed equations (8)-(10) are solved analytically using ADM. The methodology for the proposed problem is elaborated as follows:

To re-write equations (8)-(10), we introduced the operator $\Re = \frac{d^2}{d\xi^2}(\bullet)$ with an inverse operator $\Re^{-1}(\bullet) = \int_0^\xi\int_0^\xi(\bullet)\,d\xi d\xi.$ Therefore, the set of equations (8)-(10) is presented as:

$$\left.\begin{aligned}&\Re(F) = (\operatorname{Re} F' + (M+Da)F - \lambda_1\theta - \lambda_2\phi - P)((1-n) + nWeF')^{-1},\\&\Re(\theta) = \Pr(\operatorname{Re}\theta' - (S+I)\theta - EcF'^2 - (M+Da)EcF^2 - Nb\theta'\phi' - Nt\theta'^2),\\&\Re(\phi) = K\,Le\Pr\phi - \tfrac{Nt}{Nb}\Re(\theta)\end{aligned}\right\} \tag{16}$$

Taking the inverse of the above equations, we arrive at the following,

$$\left.\begin{aligned}&F(\xi) = \Re^{-1}\{(\operatorname{Re} F' + (M+Da)F - \lambda_1\theta - \lambda_2\phi - P)((1-n) + nWeF')^{-1}\},\\&\theta(\xi) = \Re^{-1}\{\Pr(\operatorname{Re}\theta' - (S+I)\theta - EcF'^2 - (M+Da)EcF^2 - Nb\theta'\phi' - Nt\theta'^2)\},\\&\phi(\xi) = \Re^{-1}\left\{K\,Le\Pr\phi - \tfrac{Nt}{Nb}\Pr(\operatorname{Re}\theta' - (S+I)\theta\right.\\&\qquad\qquad\left. - EcF'^2 - (M+Da)EcF^2 - Nb\theta'\phi' - Nt\theta'^2)\right\},\end{aligned}\right\} \tag{17}$$

Series expansion of all the linear and nonlinear terms of equation (17) are considered as,

$$\left.\begin{aligned}&F = \sum_{k=0}^{\infty} A_k, F' = \sum_{k=0}^{\infty} B_k, F^2 = \sum_{k=0}^{\infty} C_k, F'^2 = \sum_{k=0}^{\infty} D_k, \theta = \sum_{k=0}^{\infty} E_k,\\&\theta' = \sum_{k=0}^{\infty} F_k, \phi = \sum_{k=0}^{\infty} G_k, \theta'\phi' = \sum_{k=0}^{\infty} H_k, \theta'^2 = \sum_{k=0}^{\infty} I_k\end{aligned}\right\} \tag{18}$$

The initial guess solutions are obtained from the given initial conditions presented in equation (11), and these are,

$$F_0(\xi) = (S_v + \xi)F'(0), \theta_0(\xi) = \theta(0) + B_i(\theta(0) - 1)\xi, \phi_0(\xi) = \phi'(0)\xi \tag{19}$$

The recursive expressions become

$$\left.\begin{aligned}&F_{k+1}(\xi) = \Re^{-1}\{(\operatorname{Re} B_k + (M+Da)A_k - \lambda_1 E_k - \lambda_2 G_k - P)((1-n) + nWeB_k)^{-1}\},\\&\theta_{k+1}(\xi) = \Re^{-1}\{\Pr(\operatorname{Re} A_k - (S+I)E_k - EcD_k - (M+Da)EcC_k - NbH_k - NtI_k)\},\\&\phi_{k+1}(\xi) = \Re^{-1}\left\{K\,Le\Pr G_k - \tfrac{Nt}{Nb}\Pr(\operatorname{Re} A_k - (S+I)E_k\right.\\&\qquad\qquad\left. - EcD_k - (M+Da)EcC_k) - NbH_k - NtI_k\right\},\end{aligned}\right\} \tag{20}$$

$k = 0, 1, 2, \ldots$ The unknowns are numerically evaluated, and the approximate analytical solutions for different flow profiles can be obtained further.

5. Discussion on the present outcomes

The influence of free convection on the three-dimensional flow of tangent hyperbolic nanofluid through a microchannel in the occurrence of the transverse magnetic field is presented in this article. The flow through a porous medium for the interaction of dissipative heat, thermal radiation, and heat source affects the flow phenomena greatly. Also, due to the variation of Brownian and thermophoresis, the two-phase nanofluid model contributes significantly to the coupled heat and solutal transport properties. More importantly, the transformed governing equations formulated by including several characterizing parameters are handled analytically by implementing the Adomian Decomposition method. The behaviour of the several physical components affecting the flow phenomena is displayed in Figs.2-12 and the computational results for the rate coefficients are also deployed in tabular form. The following fixed values of the parameters are presented during the entire computation process $n=0.5,\ We=0.5,\ Re=2,\ M=1,\ Da=1,\ \lambda_1=0.01, \lambda_2=0.01,\ P=1,$ $Pr=2,\ S=0.1,\ I=0.1,\ Ec=0.1,\ S_v=0.5,\ Bi=0.50,\ Nb=0.5,\ Nt=0.5,$ $Le=1,$ and $K=2$ consider the particular variation as displayed in the corresponding figures.

Figure 2 illustrates the characteristic of the non-Newtonian Weissenberg number and the Reynolds number on the velocity profiles. The Weissenberg number exhibits the flow phenomena as an elastic force to the viscous force. It is expressed as the relationship between stress relaxation time with respect for the specific process time. Enhanced We suggests the increasing elastic force overrides viscous force, resulting in the increased fluid velocity near the upper plate. The minor enhancement near the lower plate of the channel retards the channel width gradually.

Further, the application of the Reynolds number plays an important role in fluid velocity. Mathematically, it is expressed as the ratio of inertial and viscous forces. Here, the dominating nature of the viscous force over the inertial force enhances the Reynolds number. Therefore, increasing the Reynolds number, the fluid velocity closer to the lower plate became deviating from their position for which the channel width increases, but at the middle layer of the channel, the hike in the profile is maximum.

Figure 3 exhibits the impact of the magnetic parameter in conjunction with the porous matrix affecting the fluid velocity. The impact of magnetization is due to the Interaction of a transverse uniform magnetic field on the flow phenomena. The conjunction of this vector field produces a resistive force termed “Lorentz force” that tends to retards the fluid velocity; the property also shows greater retardation in the fluid velocity near the lower plate region. Further, as described in the magnetic case, porosity is also exhibited as a resistive force, and a stronger deceleration in the fluid velocity is exhibited due to increased porosity. The observation clarifies that the flow through the impermeable medium shows its maximum strength compared to the flow through a porous medium.

Figure 4 displays the variation of buoyant forces due to the involvement of the thermal and solutal buoyancy on the fluid velocity. The variation shows the negative and the positive values, where the negative indicates the heating of the plate and the positive stands for the cooling. The mathematical expression gives rise to the physical significance of the buoyancy parameter, and the cooling of the plate means the ambient state temperature is greater; therefore, the temperature flow is towards the plate, and the reverse condition is deployed in case of heating. This indicates that with increasing buoyancy, the fluid temperature increases.

Figure 5 shows the effectiveness of the parameters like the magnetic and porosity on the fluid temperature exhibiting resistivity properties. The behaviour of the resistive forces decelerates the fluid velocity significantly, and at a similar instant, it is observed that the energy stored near the surface is at the lower plate of the channel. This stored energy boosts the fluid temperature, transferring energy from the lower region to the upper. Also, it is an exhibit that permeability enriches the fluid temperature within the fluid domain. This enhancement is due to the resistivity property of including the porous matrix.

Figure 6 shows the impact of the thermophoresis and the Brownian motion on the fluid temperature distribution for the existence of other characterizing parameters. Both parameters exist due to the inclusion of the terms $Nb\phi'\theta'$ and $Nt\theta'^2$ equation (9) that enriches the flow properties. The combined effect of Brownian and thermophoresis is due to the cross-diffusion between the thermal and solutal gradients. The observation signifies that the enhanced thermophoresis and Brownian encourage the flow phenomenon of the fluid temperature near the lower plate, whereas the reverse impact is rendered in the case of Brownian motion at the upper plate.

Figure 7 exhibits the behaviour of the Eckert number and the power law index parameter on the fluid temperature distribution of the non-Newtonian fluid. The Eckert number exists because of the coupling effect of the velocity and temperature for the interaction of the dissipative heat. The inclusion of the magnetic and porosity suggests the behaviour of all the dissipative energy that affects the flow properties. The enhanced Eckert number is due to the retardation in the temperature difference between the fluid and the ambient state. Here, the enhanced Eckert number enriches the nanofluid temperature throughout the domain. A similar impact is rendered for the index parameter.

Figure 7 represents the physical behaviour of the thermal Biot number and the Reynolds number affecting the fluid temperature. The Biot number exists because of the convective boundary condition applied in the heat transport phenomenon. The property of the Biot number reveals that the increasing Biot number enhances the fluid temperature, and this augmentation is exhibited towards the upper plate region. The enhancement effect is due to the stored energy near the lower plate region enchasing heat energy and the flow towards the upper plate region. Further, the increasing Reynolds number also enhances the fluid temperature throughout.

Figure 8 reveals the impact of the additional heat source and the radiative heat affecting the nanofluid temperature profiles. The basic idea behind including thermal radiation is to measure the amount of electromagnetic radiation emitted from the fluid element. This emission causes cooling in the lower plate region; therefore, the fluid temperature greatly enhances. Thus, it is observed that the increasing thermal radiation augments the nanofluid temperature significantly. Further, the additional heat source also presents a favourable condition for smooth enhancement in the temperature distribution.

Figure 9 portrays the behaviour of the Lewis number on the fluid concentration profile in conjunction with the impact of the Reynolds number. The mathematical description of the Lewis number exhibits that it is the ratio of the diffusivity forces like thermal and Brownian diffusivity. The enhanced Lewis number clarifies that the Brownian diffusivity, i.e., the intermolecular forces between the fluid elements retards. Therefore, the thermal diffusivity enhances, and this physical property reveals significant retardation in the fluid concentration. The behaviour of the Reynolds number reveals that the fluid concentration enriches the domain.

Figure 10 depicts the characteristic of the Brownian and thermophoresis parameters on the fluid concentration. The significant role of these parameters was exhibited in the fluid temperature, and the dual behaviour is exhibited with their increasing values. The figure reveals that the enhanced Brownian motion enriches the concentration because of its random movement within the domain. The opposite impact is presented on the concentration profile for the enhanced thermophoresis parameter.

Figure 11 shows the characteristic of the chemical reaction parameter on the fluid concentration distribution. The negative value of the reactant reveals the constructive form of the chemical substances, whereas the positive represents the destructive reaction. Also, the profile exhibits the behaviour for the non-occurrence of the reacting agents. It is exhibited that with the increasing chemical reaction from constructive to destructive the fluid concentration retards, and this retardation is towards the upper plate domain. The behaviour shows its linearity due to the absence of the chemical reaction parameter.

Finally, the simulated results of the rate coefficients, such as the shear rate and the heat and solutal transfer rate for the various parameters characterizing the flow phenomena, are presented in Table 2 and Table 3, respectively. Table 2 shows that with the increasing index parameter and the Reynolds number, the rate coefficient for the shear rate retards in magnitude significantly. Further, the non-Newtonian parameter for the impact of the Weissenberg number and the buoyant forces favours enhancing smoothly. The increase in the resistive force for the impact of magnetic and porosity, along with the slip parameter retards the shear rate coefficient. Table 3 shows that the enhanced values of the Eckert number, thermal radiation, additional heat source, Brownian and thermophoresis parameters encourage the heat transfer rate coefficient at both plates. However, the augmentation in the Biot number encourages it significantly. The increasing Lewis number and the chemical reaction parameter decelerate the solutal transfer rate.

6. Conclusive remarks

The free convection of tangent hyperbolic nanofluid flow through a parallel channel embedding within a porous matrix is investigated in the present article. The dissipative heat composed of viscous, Joule and Darcy parameters is included due to the iteration of the resistive force offered by magnetic and porosity. The novelty arises because of the behaviour of Brownian motion and thermophoresis, thermal radiation, heat source, and chemical reaction. Finally, the important outcomes of the study are visualized as follows;

- The influence of the non-Newtonian Weissenberg number is to enhance the fluid velocity at the upper plate, whereas the increasing Reynolds number has a reverse impact on the velocity distribution.
- The enhanced buoyancy forces for the augmentation in the thermal and solutal buoyancy further enrich the fluid velocity throughout the domain; the cooling case dominates the heating of the plate.

- The resistivity due to the inclusion of magnetic parameters in the presence of the porous matrix is favourable for the smooth enhancement in the channel width near the lower plate region.
- The higher values of the Biot number for the influence of convective heat boundary condition augments the fluid temperature, and a hike is remarked at the central region of the channel further; the increasing heat source and thermal radiation enhances it significantly.
- The Brownian motion and thermophoresis exhibit their dual characteristic on the fluid concentration distribution, and it is seen that the increasing Brownian motion enriches the profile, whereas thermophoresis decelerates it.
- The shear rate retards in magnitude for the increasing Reynolds number; further, the non-Newtonian parameter, Weissenberg number and the buoyant forces significantly enhance it.

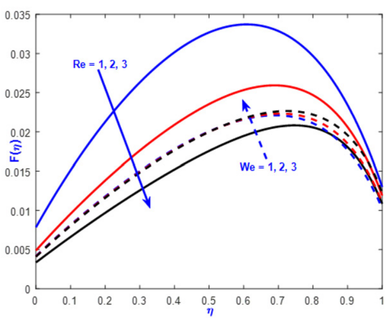

Figure 2

Role of *Re* and *We* on fluid Velocity

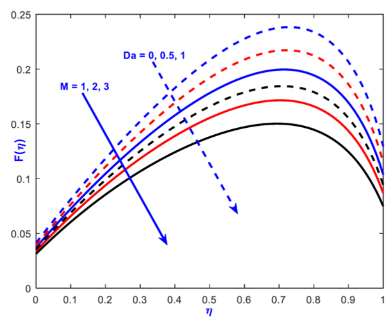

Figure 3

Role of *M* and *Da* on fluid Velocity

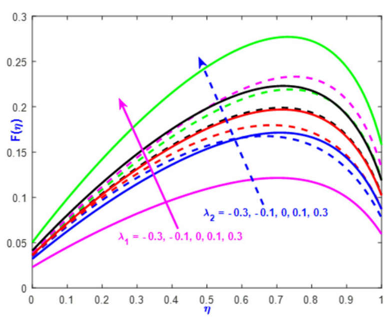

Figure 4

Role of λ_1 and λ_2 on fluid Velocity

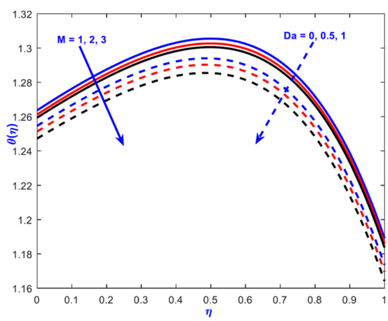

Figure 5

Role of *M* and *Da* on fluid Temperature

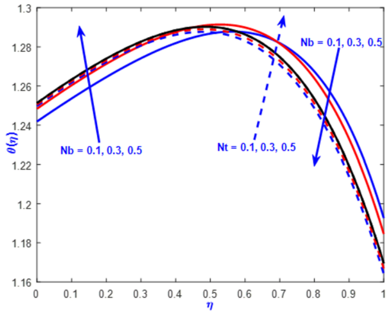

Figure 6

Role of *Nb* and *Nt* on fluid Temperature

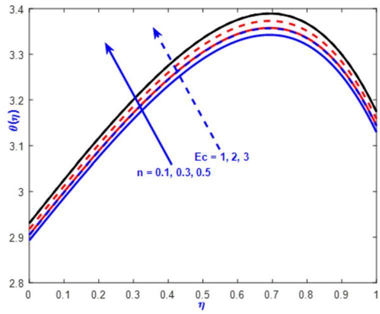

Figure 7

Role of *n* and *Ec* on fluid Temperature

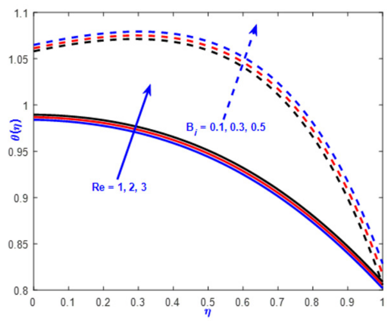

Figure 8

Role of *Re* and B_i on fluid Temperature

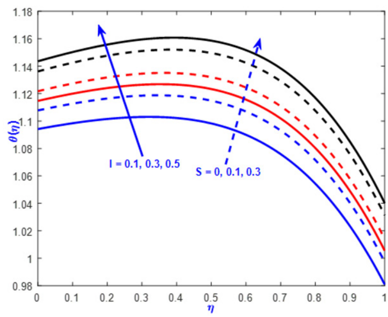

Figure 9

Role of *I* and *S* on fluid Temperature

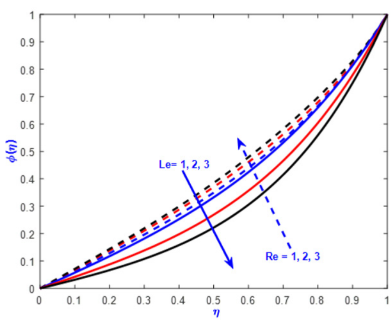

Figure 10

Role of *Le* and *Re* on fluid Concentration

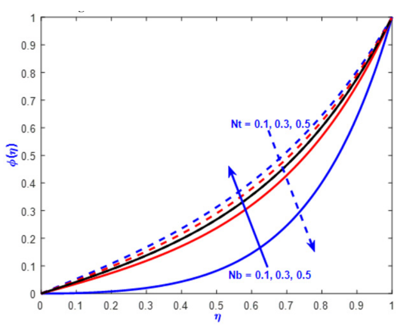

Figure 11

Role of *Nb* and *Nt* on fluid Concentration

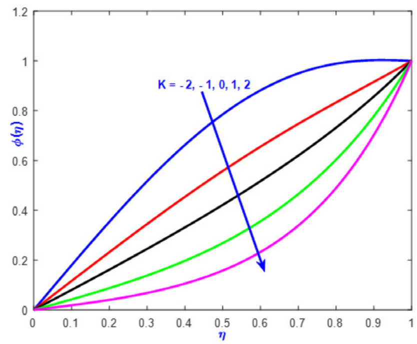

Figure 12

Role of K on fluid Concentration

Table 2

Numerical Computation of Shear rate

N	Re	We	M	Da	P	λ_1	λ_2	S_v	Cf_0 Cf_1
0.5	2	0.5	1	1	1	0.01	0.01	0.5	0.1549 -0.2070
0.1									0.2297 -0.3069
0.2									0.2135 -0.2882
0.5	1								0.1957 -0.2134
	3								0.1233 -0.1921
	2	0.2							0.1499 -0.2204
		0.3							0.1516 -0.2160
		0.5	2						0.1291 -0.1707
			3						0.1110 -0.1446
			1	2					0.1291 -0.1707
				3					0.1110 -0.1446
				1	-1				0.1548 -0.2070
					2				0.1549 -0.2070
					1	0.2			0.1946 -0.2496
						0.3			0.2163 -0.2713
						0.5	0.2		0.1582 -0.2198
							0.3		0.1600 -0.2265
							0.5	0.2	0.1881 -0.3086
								0.3	0.1757 -0.2627

Table 3

Numerical Computation of the rate of heat transfer and rate of solutal transfer

n	Re	M	Da	Pr	Ec	S	I	Nb	Nt	B_i	Le	K	Nu_0	Nu_1	Sh_0	Sh_1
0.5	2	1	1	2	0	0.01	0.01	0.5	0.5	0.5	1	2	-0.1270	-0.5861	-0.4125	2.4907
0.1													-0.1240	-0.5822	-0.4131	2.4858
0.2													-0.1247	-0.5831	-0.4130	2.4869
0.5	1												-0.1180	-0.5325	-0.3411	2.3521
	3												-0.0878	-0.5662	-0.4705	2.5256
	2	2											-0.1259	-0.5847	-0.4131	2.4892
		3											-0.1249	-0.5836	-0.4134	2.4878
		1	2										-0.1259	-0.5847	-0.4131	2.4892
			3										-0.1249	-0.5836	-0.4134	2.4878
			1	1									-0.0157	-0.4356	-0.5843	1.8349
				6									-0.1521	-0.6776	-0.1916	4.0769
				2	0								-0.1189	-0.5760	-0.4150	2.4786
					0.1								-0.1199	-0.5772	-0.4147	2.4801
					0.2	0.2							-0.0621	-0.5081	-0.4378	2.4041
						0.3							-0.0693	-0.5168	-0.4350	2.4137
						0.01	0.02						-0.2402	-0.7223	-0.3689	2.6421
							0.03						-0.4232	-0.9422	-0.2980	2.8862
							0.01	0.2					-0.1240	-0.5960	-0.2587	3.2157
								0.3					-0.1255	-0.5936	-0.3448	2.8156
								0.5	0.2				-0.1264	-0.5841	-0.4951	2.2390
									0.3				-0.1266	-0.5848	-0.4674	2.3222
									0.5	0.2			-0.2703	-0.4821	-0.4125	2.5233
										0.3			-0.1729	-0.4696	-0.4296	2.4537
										0.5	2		-0.1197	-0.5734	-0.2318	3.1878
											3		-0.1157	-0.5655	-0.1346	3.7579
											1	-2	-0.1270	-0.5861	-0.4125	2.4907
												-1	-0.1270	-0.5861	-0.4125	2.4907
												1	-0.1270	-0.5861	-0.4125	2.4907

Appendix

Nomenclature

B_0	magnetic flux density
Le	Lewis number
C	concentration of species
Sh	Sherwood number
C_p	specific molecular diffusivity
T	fluid temperature
C_∞	species concentration at infinity
T_∞	fluid temperature at infinity
D	chemical molecular diffusivity
v_0	scale of suction velocity
Da	Darcy number

Greek symbols

Ec	Eckert number
η	similarity variable
F	radiation parameter
ρ	density of the fluid
g	acceleration due to gravity
μ	dynamic viscosity
Gm	solutal Grashof number
ν	kinematic viscosity
Gr	thermal Grashof number
κ	thermal conductivity
K	chemical reaction parameter
β_T	coefficient of thermal expansion
m	mean concentration difference
β_C	coefficient of volume expansion
M	magnetic parameter
f	dimensionless fluid velocity
Nu	Nusselt number
θ	dimensionless temperature

Pr Prandtl number
ϕ dimensionless concentration
q mean temperature difference
τ skin friction
q_r constant heat flux
σ electrical conductivity
S heat source parameter

References

[1] S.U.S. Choi, J.A. Jeffery, Enhancing thermal conductivity of fluids with nanoparticles, ASME Fluids Eng. Div. 231, 99-105 (1995).

[2] T. Hayat, M. Imtiaz, A. Ahmed, F. Alzahrani, Effects of homogeneous–heterogeneous reactions in flow of magnetite-Fe_3O_4 nanoparticles by a rotating disk, *J. Mol. Liq.* 216, 845-855 (2016).

[3] M. Sheikholeslami, CuO-water nanofluid flow due to magnetic field inside a porous media considering Brownian motion, *J. Mol. Liq*. 249, 921-929 (2018).

[4] A.J. Chamkha, S. Abbasbandy, A.M. Rashad, Non-Darcy natural convection flow of non-Newtonian nanofluid over a cone saturated in a porous medium with uniform heat and volume fraction fluxes, *Int. J. Numer. Methods Heat Fluid Flow* 25, 422-437 (2015).

[5] A.J. Chamkha, A.M. Aly, MHD free convection flow of a nanofluid past a vertical plate in the presence of heat generation or absorption effects, Chem. Eng.Commun. 198, 425-441 (2011).

[6] T. Hayat, S Qayyum, M. Imtiaz, F. Alzahrani, A. Alsaedi, Partial slip effect inflow of magnetite-Fe_3O_4 nanoparticles between rotating stretchable disks, *J.Magn. Magn. Mater*. 413, 39-48 (2016).

[7] M. Sheikholeslami, D.D. Ganji, M.M. Rashidi, Magnetic field effect on unsteady nanofluid flow and heat transfer using Buongiorno model, *J. Magn. Magn.Mater*. 416, 164-173 (2016).

[8] M. Sheikholeslami, D.D. Ganji, Free convection of Fe3O4-water nanofluid under the influence of an external magnetic source, *J. Mol. Liq*. 229, 530-540 (2017).

[9] M. Sheikholeslami, D.D. Ganj, Transportation of MHD nanofluid free convection in a porous semi annulus using numerical approach, Chem. Phys. Lett. 669, 202-210 (2017).

[10] M.M. Bhatti, S.R. Mishra, A. Shaid, S. Jena, Buoyancy driven chemicalized EMHD nanofluid flow through a stretching plate with Darcy-Brinkman-Forchheimer porous medium, Heat Transfer Research 11, 1105-1126 (2019).

[11] S. Jena, D.K. Mohapatra, S.R. Mishra, Cu-water and Cu-kerosene micropolar nanofluid flow over a permeable stretching sheet, Heat Transfer—Asian Research 48, 2478-2496 (2019).

[12] S. Jena, S.R. Mishra, P.K. Pattnaik, R.P. Sharma, The nanofluid flow between parallel plates and heat transfer in presence of chemical reaction and porous matrix, *Latin American Applied Research-An International Journal*, 50, 283-289 (2020).

[13] R.U. Haq, F.A. Soomro, Z. Hammouch, Heat transfer analysis of CuO-water enclosed in a partially heated rhombus with heated square obstacle, *Int. J. Heat Mass Transf*. 118, 773-784 (2018).

[14] R. Ahmad, M. Mustafa, T. Hayat, A. Alsaedi, Numerical study of MHD nanofluid flow and heat transfer past a bidirectional exponentially stretching sheet, *J. Magn. Magn. Mater.* 407, 69-74 (2016).

[15] G.K. Ramesh, T. Hayat, A. Alsaedi, Stagnation point flow of Maxwell fluid towards a permeable surface in the presence of nanoparticles, *Alexandria Eng. J.* 55, 857-865 (2016).

[16] M. M. Bhatti, T. Abbas, & M. M. Rashidi, Entropy generation as a practical tool of optimization for non-Newtonian nanofluid flow through a permeable stretching surface using SLM, *Journal of Computational Design and Engineering*, 4, 21-28 (2017).

[17] A.K. Mishra, P.K. Pattnaik, S.R. Mishra, N. Senapati, Dissipative heat energy on Cu and Al_2O_3 ethylene–glycol-based nanofluid flow over a heated semi-infinite vertical plate, *Journal of Thermal Analysis and Calorimetry,* 145(6) (2020). doi: 10.1007/s10973-020-09666-z

[18] S. Jena, S. R. Mishra, P.K. Pattnaik, R.P. Sharma, Nanofluid flow between parallel plates and heat transfer in presence of chemical reaction and porous matrix, Latin American Applied Research, 50(4), 283-289 (2020).

[19] S.K. Parida, S.R. Mishra, R.K. Dash, P.K. Pattnaik, M. Khan, Y.-M. Chu, F. Shah, Dynamics of dust particles in a conducting water based kerosene nanomaterials: A computational approach, *International Journal of Chemical Reactor Engineering,* 19(8) (2021). doi: 10.1515/ijcre-2020-0204

[20] B. Mohanty, S. Jena, P.K. Pattnaik, MHD Nanofluid Flow over stretching/Shrinking Surface in Presence of Heat Radiation Using

Numerical Method, *International Journal on Emerging Technologies* 10(2b), 119-125 (2019).

[21] P.K. Pattnaik, and T. Biswal, Analytical solution of MHD free convective flow through porous media with time-dependent temperature and concentration, *Walailak J. of Sci & Tech*, 12(9), 749-762 (2015).

[22] S.R. Mishra, P.K. Pattnaik, M.M. Bhatti, T Abbas, Analysis of heat and mass transfer with MHD and chemical reaction effects on viscoelastic fluid over a stretching sheet, *Indian Journal of Physics,* 91 (10), 1219-1227 (2017).

[23] P.K. Pattnaik, S.R. Mishra, A.K. Barik, A.K. Mishra, Influence of chemical reaction on magnetohydrodynamic flow over an exponential stretching sheet: a numerical study, *International Journal of Fluid Mechanics Research*, 47(2), 1-12 (2020).

[24] P.K. Pattnaik, S. Jena, A. Dei, G. Sahu, Impact of chemical reaction on micropolar fluid past a stretching sheet, *JP Journal of Heat and Mass Transfer*, 18 (1), 207-223 (2019).

[25] P.K. Pattnaik, S.R. Mishra, B. Mahanthesh, B.J. Gireesha and M.R. Gorji, Heat transport of nano-Micropolar fluid with an exponential heat source on a convectively heated elongated plate using Numerical computation, Multidiscipline Modeling in Materials and Structures, 16(5), 1295-1312 (2020). doi: 10.1108/MMMS-12-2018-0222.

[26] A.K. Barik, S.K. Mishra, S.R. Mishra and P.K. Pattnaik, Multiple Slip effects on MHD nanofluid flow over an inclined, radiative and chemically reacting stretching sheet by means of FDM, Heat transfer Asian Research, 49(1), 477-501 (2020). doi: 10.1002/htj.21622.

[27] S.R. Mishra, P.K. Pattnaik, G.C. Dash, Effect of heat source and double stratification on MHD free convection in a micropolar fluid, *Alexandria Engineering Journal*, 54(3), 681-689 (2015).

[28] S.R. Mishra, B. Mahanthesh, J. Mackolil, P.K. Pattnaik, Nonlinear radiation and cross-diffusion effects on the micropolar nanoliquid flow past a stretching sheet with an exponential heat source, Heat transfer Asian Research, 50(4), 3530-3546 (2021).

[29] B. Ali, P.K. Pattnaik, R.A. Naqvi, H. Waqas, S. Hussain, Brownian motion and thermophoresis effects on bioconvection of rotating Maxwell nanofluid over a Riga plate with Arrhenius activation energy and Cattaneo–Christov heat flux theory, Thermal Science and Engineering Progress, 23, 100863 (2021).

[30] P.K. Pattnaik, D.K. Mohapatra, S.R. Mishra, Influence of Velocity Slip on the MHD Flow of a Micropolar Fluid over a Stretching Surface, Lecture Notes in Mechanical Engineering, 307-321 (2021).

[31] P.K. Pattnaik, J.R. Pattnaik, S.R. Mishra, K.S. Nisar, Variation of the shape of Fe_3O_4-nanoparticles on the heat transfer phenomenon with the inclusion of thermal radiation, *Journal of Thermal Analysis and Calorimetry*, (2021). doi: 10.1007/s10973-021-10605-9

[32] P. K. Pattnaik, S.R. Mishra, M. M. Bhatti, Duan–Rach approach to study Al_2O_3-ethylene glycol $C_2H_6O_2$ nanofluid flow based upon KKL model, Inventions, 5(3), 45 (2020).

[33] A.J. Chamkha, S. Abbasbandy, A.M. Rashad, K. Vajravelu, Radiation effects on mixed convection about a cone embedded in a porous medium filled with a nanofluid, Meccanica, 48, 275-285 (2013).

[34] A.J. Chamkha, A.A. Khaled, Similarity solutions for hydromagnetic mixed convection heat and mass transfer for Hiemenz flow through porous media, *International Journal of Numerical Methods for Heat & Fluid Flow,* 10, 94-115 (2000).

[35] C.L. Cogley, W.G. Vincenti, E.S. Gilles, Differential approximation for radiative heat transfer in a non-grey gas near equilibrium. American Institute of Aeronautics and Astronautics, 6(3), 551-553 (1968).

[36] F. White, Viscous Fluid Flow. 3rd ed. New York: McGraw-Hill; (2006).

[37] C. Kleinstreuer, Engineering Fluid Dynamics. Cambridge: Cambridge University Press; (1997)

[38] Amit Kumar Gupta, Pushpa Gothwal, Dinesh Goyal & Carlos M. Travieso-Gonzalez. IoT-Galvanized pandemic special E-Toilet for generation of sanitized environment, *Journal of Discrete Mathematical Sciences and Cryptography* (2022), DOI: 10.1080/09720529.2022.2068607.

[39] Amit Kumar Gupta, Vijander Singh, Priya Mathur & Carlos M. Travieso-Gonzalez. Prediction of COVID-19 pandemic measuring criteria using support vector machine, prophet and linear regression models in Indian scenario, *Journal of Interdisciplinary Mathematics* (2020), DOI: https://doi.org/10.1080/09720502.2020.1833458.

[40] Jitendra Singh Yadav, Amit Kumar Gupta & Arjit Saxena. A review on gender identification using machine learning based on fingerprints, *Journal of Information and Optimization Sciences* (2019), 40:5, 1121-1129, DOI: https://doi.org/10.1080/02522667.2019.1638002.